© 2014. Published by The Company of Biologists Ltd | Development (2014) 141, 2302-2312 doi:10.1242/dev.101667

RESEARCH ARTICLE

Fate map of the chicken otic placode

Luis Óscar Sánchez-Guardado[1], Luis Puelles[2] and Matías Hidalgo-Sánchez[1,*]

ABSTRACT

The inner ear is an intricate three-dimensional sensory organ that arises from a flat, thickened portion of the ectoderm termed the otic placode. There is evidence that the ontogenetic steps involved in the progressive specification of the highly specialized inner ear of vertebrates involve the concerted actions of diverse patterning signals that originate from nearby tissues, providing positional identity and instructive context. The topology of the prospective inner ear portions at placode stages when such patterning begins has remained largely unknown. The chick-quail model was used to perform a comprehensive fate mapping study of the chick otic placode, shedding light on the precise topological position of each presumptive inner ear component relative to the dorsoventral and anteroposterior axes of the otic placode and, implicitly, to the possible sources of inducing signals. The findings reveal the existence of three dorsoventrally arranged anteroposterior domains from which the endolymphatic system, the maculae and basilar papilla, and the cristae develop. This study provides new bases for the interpretation of earlier and future descriptive and experimental studies that aim to understand the molecular genetic mechanisms involved in otic placode patterning.

KEY WORDS: Otic specification, Morphogenesis, Sensory patch, Maculae, Cristae, Semicircular canals, Endolymphatic system, Tegmentum vasculosum, Compartment, Cell lineage

INTRODUCTION

Modeling any developing organ of an organism is an attempt to rationally systematize a complex network of molecular and cellular interactions. It has been shown that self-enhancement and long-range inhibition mechanisms can control position-dependent gene activations and repressions in pattern-forming systems (Meinhardt, 2008), managing cell segregation mechanisms devoted to the creation of lineage compartments in growing tissues (Dahmann and Basler, 1999). The vertebrate inner ear is one of the most intricate examples of organogenesis, and is an excellent model for scientific inquiry into the molecular kit implemented in complex sensory organogenesis. This elaborate sensory organ arises from the otic placode, a thickened, two-dimensional portion of ectoderm located on each side of the developing hindbrain, dorsal to the pharyngeal branchial pouches. The otic placode invaginates and pinches off from surface ectoderm to form a simple saccular otocyst which, after diverse inductive and morphogenetic events, then gives rise to the three-dimensional inner ear complex, comprising an interconnected epithelial labyrinth with vestibular and auditory sensory specializations. The vestibular part is composed of utricle, saccule, three semicircular canals (with the respective macular and ampullary sensory organs) plus the non-sensory endolymphatic system, while the auditory part forms the cochlea. The corresponding sensory ganglion cells are produced locally as well.

The morphogenesis of this organ is governed by signals diffusing from nearby tissues, or spreading planarly within the otic epithelium itself. Despite various breakthroughs in the molecular genetic mechanisms involved in the specification and shaping of the membranous labyrinth, many questions remain about its early patterning, which might start as early as the placodal stage. Thus, it would be very useful to construct precise fate maps that relate the otic placode to the derived regionalized vesicle.

A few fate mapping studies have been carried out on the developing vertebrate inner ear, mostly using the chick embryo as a model. These works used either injections of the fluorescent lipophilic vital dyes DiI/DiO or retrovirus-mediated lineage analysis (Abelló et al., 2007; Bell et al., 2008; Brigande et al., 2000a; Kil and Collazo, 2001; Kozlowski et al., 1997; Lang and Fekete, 2001; Li et al., 1978; Pieper et al., 2011; Satoh and Fekete, 2005; Stevenson et al., 2012; Streit, 2002; Xu et al., 2008). Some of the studies were performed before the otic and trigeminal placodes were constituted as two separate identities (Kozlowski et al., 1997; Pieper et al., 2011; Streit, 2002), and a single study of the frog inner ear was carried out exactly at the otic placode stage (Kil and Collazo, 2001). Other studies addressed otic cup stages (Abelló et al., 2007; Bell et al., 2008; Brigande et al., 2000a) or otocyst stages (Kil and Collazo, 2001; Li et al., 1978), i.e. examined otic primordia that had already initiated important morphogenetic changes. The resulting differences in methods and data sets have generated some unresolved questions, such as the possible existence of compartments or of cell lineage dispersion within the otic epithelium (Bell et al., 2008; Kil and Collazo, 2002).

Here, we present a detailed fate mapping study of the avian otic placode at the 10-somite stage, using the well-known chick-quail grafting model (Alvarado-Mallart and Sotelo, 1984; Le Douarin, 1969), with an experimental operating grid of 12 sectors [three square dorsoventral (DV) areas each at four anteroposterior (AP) levels, using neighboring hindbrain rhombomeres as positional landmarks; Vaage, 1969]. The fates were evaluated at stages HH29-HH34 using various specific markers. The relative topological position of the presumptive territory for all sensory and non-sensory components of the membranous labyrinth could thus be identified. We found that the avian otic placode is constituted by three band-like AP domains arranged dorsoventrally. The dorsalmost domain gives rise to the endolymphatic system, whereas the ventralmost band develops into the ampullary cristae and associated semicircular canals. The intermediate domain generates the maculae and the macular-derived basilar papilla, together with their attached non-sensory epithelia. This detailed fate map should be of help in the search for a model that considers dose-dependent and multi-step actions of diverse inductive signals released from nearby tissues, to achieve the proper specification of each constituent part of the avian inner ear in a mosaic-like fashion.

[1]Department of Cell Biology, Faculty of Science, University of Extremadura, 06071 Badajoz, Spain. [2]Department of Human Anatomy and Psychobiology, School of Medicine, University of Murcia, 30003 Murcia, Spain.

*Author for correspondence (mhidalgo@unex.es)

Received 29 July 2013; Accepted 1 April 2014

Development (2014) 141, 2302-2312 doi:10.1242/dev.101667

RESULTS

Grafting experiments

To obtain a detailed fate map of the otic placode at the 10-somite stage, we first analyzed the possible contribution of a broad portion of the cephalic ectoderm to the otic placode (Fig. 1A). Preliminary homotopic quail-chick grafts of large pieces of embryonic skin next to particular rhombomeres (rh) showed that only the ectoderm facing rh4 to prospective rh7 contributes to the inner ear (Fig. 1A). To analyze with greater resolution the fate of the portions of ectoderm associated topographically with each of these rhombomeres, three types of grafting experiments were performed at each of these four AP sites (Fig. 1A,B). In all cases, the dorsal border of the grafted territory coincided with the embryonic midline (Fig. 1A). Type 1 grafts were limited to the dorsal third of the ectodermal strip at each AP level (dT; Fig. 1A,B). Type 2 grafts included the dorsal two-thirds of the respective tissue strips at each level, therefore including the type 1 graft domain (Fig. 1A,B). The consequently expanded extent of type 2 grafted territories was analyzed at the same stages, noting differences with type 1 grafts. The supplementary quail-derived area was assigned to the fate of the middle third of the grafted ectoderm (mT; Fig. 1B). Type 3 grafts comprised the entire cephalic ectoderm next to a specific rhombomere, thus encompassing the territories already taken in grafts of types 1 and 2, plus a further ventral domain. Comparing the type 2 and type 3 grafts, the supplementary QCPN-positive territory was associated with the fate of the ventral third of the relevant transverse strip (vT; Fig. 1B). The fate map we obtained is thus based on otic-derived structure determined at stages HH29-HH34, projected backwards upon a 4×3 grid of square areas, adjacent to rh4-rh7 at stage HH10.

The fate of the ectoderm opposite rh4

First, the dorsal third of the ectoderm facing rh4 was transplanted (rh4-ect type 1; *n*=5; Fig. 2A). In an E6 (HH29) chimeric inner ear, the QCPN-positive quail cells were mostly localized in the anterolateral portion of the endolymphatic sac and duct, forming a DV band (Fig. 2B-D). Grafted cells were also observed in a small area immediately rostral to the endolymphatic duct insertion, in the dorsal aspect of the vestibule, far from the anterior and posterior cristae (Fig. 2E). Ventrally, the graft increased in size, extending rostrally towards the *Fgf10*-positive anterior crista (Fig. 2F), but without contacting it (Fig. 2F,G). The graft also extended ventrally toward the macula utriculi and macula sacculi. Some chimeric embryos (*n*=3/7) showed a small number of QCPN-positive cells in the dorsalmost aspect of both maculae (not shown).

Next, a type 2 graft was performed, transferring the two dorsal and middle thirds of the ectoderm facing rh4 (rh4-ect type 2; *n*=6; Fig. 2H). Grafted cells were detected in the anterolateral portion of the endolymphatic system (not shown), as already observed in rh4-ect type 1 experiments (Fig. 2B-D). In rh4 type 2 chimeric embryos, the entire macula utriculi was always occupied by QCPN-positive cells (Fig. 2I-K). Only a small portion of the utricule wall was devoid of quail cells (Fig. 2I). The lateral border of the grafted domain was commonly very near the medial limit of the lateral crista (Fig. 2I,J). The macula sacculi showed some quail cells exclusively in its dorsalmost part (Fig. 2I,J), but not in the rest of this macula (Fig. 2K). The epithelial area lying between the macula utriculi and macula sacculi was devoid of grafted cells (Fig. 2I,J).

Finally, the fate of the entire ectoderm opposite rh4 was determined (rh4-ect type 3; *n*=10; Fig. 2L), corroborating the results obtained from the previous type 2 experiments (Fig. 2H-K; dT plus mT) and deducing the fate of the remaining ventralmost portion of the grafted ectoderm (vT). In type 3 chimeric embryos, the entire wall of the utricule was now included in the transplanted area. Remarkably, the medial half of the anterior crista, but not its lateral half, was constituted by quail cells (Fig. 2M,N). The medial wall of the anterior portion of the developing vertical pouch (*a*-vp), a non-sensory structure that develops into the anterior semicircular canal, was also immunopositive for QCPN (Fig. 2M). In some cases, quail cells were also detected in the medial portion of the lateral crista (*n*=3/10; not shown; see Fig. 2O,P). The wall of the utricule was clearly constituted by grafted cells and the area between the utricular and saccular maculae was constituted by quail cells (Fig. 2O,P). Fig. 2Q,R summarizes all these results in a stage E6 inner ear.

The fate of the ectoderm opposite rh5

When the dorsal third of this ectoderm was transplanted (rh5-ect type 1; *n*=5; Fig. 3A), the quail-derived clones were observed in the

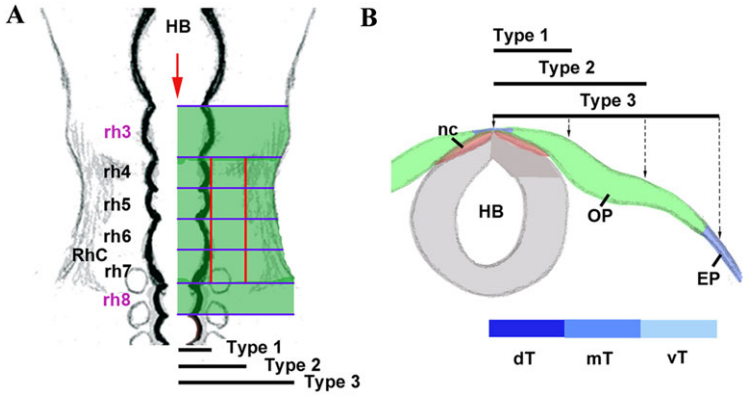

Fig. 1. Scheme of grafting experiments at the 10-somite stage. (A) Dorsal view of an avian embryo showing the graft of several portions of the cephalic ectoderm facing each rhombomere (rh) from rh3 to rh8. The horizontal blue and vertical red lines define the graft borders. Focusing on the ectoderm next to rh4, rh5 and prorhombomere C (RhC; prospective rh6 and rh7), three types of grafts were then performed for each of these anteroposterior (AP) domains: type 1 (the dorsal third of the AP ectoderm region considered), type 2 (the corresponding dorsal and intermediate thirds), and type 3 (the entire AP ectoderm region). All these graft types started dorsally at the midline of the embryos (red arrow). (B) Transverse section across the avian embryo at the level of the otic placode showing the three types of graft, with the dorsoventral (DV) thirds of the otic placode selected for grafting: dorsal third (dT), middle third (mT) and ventral third (vT). A portion of the alar plate of the neural tube was always jointly transplanted for solidity (dark gray area). HB, hindbrain; nc, neural crest; OP, otic placode; EP, epidermis.

Development (2014) 141, 2302-2312 doi:10.1242/dev.101667

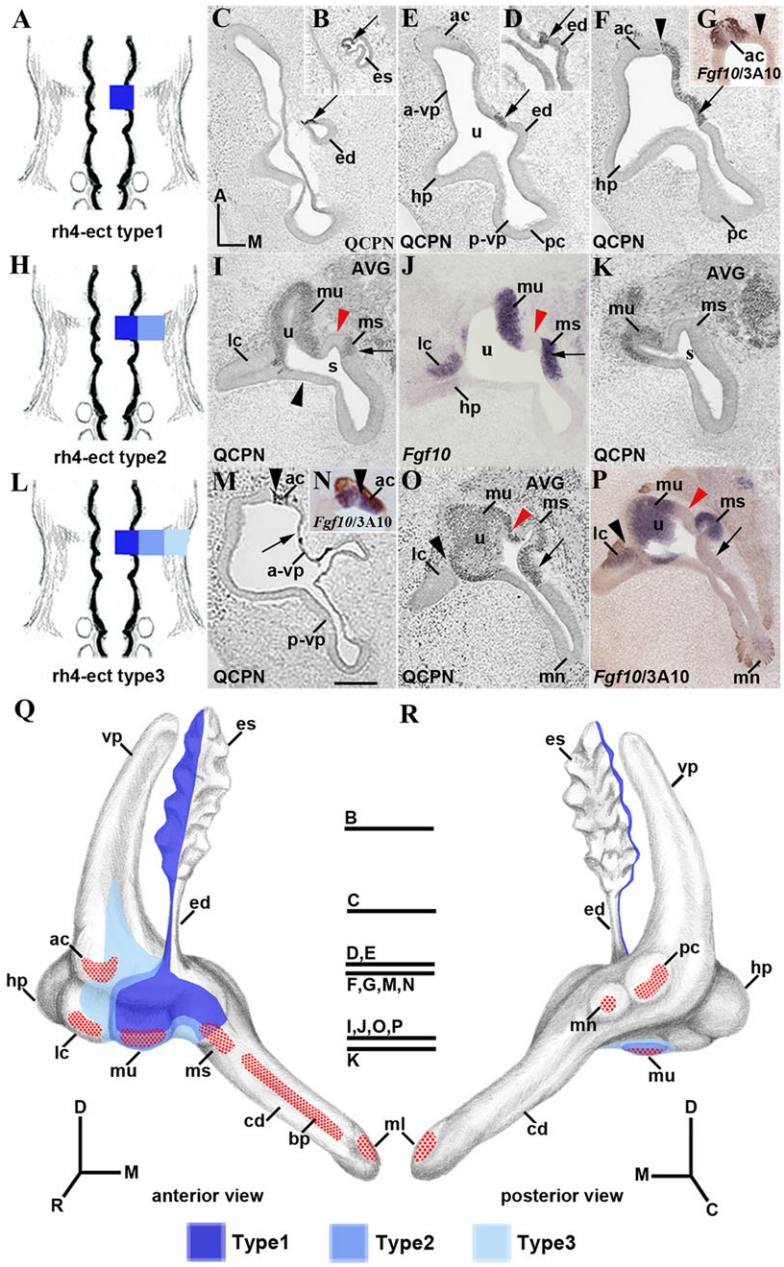

Fig. 2. Fate map of the otic placodal ectoderm facing rh4. (A) Schematic representation of the grafting results at the 10-somite stage of the rh4-ect type 1 experiment (dT; dark blue; *n*=5). (B-G) Horizontal sections through an rh4-ect type 1 chimeric embryo at stage HH29 (E6). The antibodies and probes used are indicated in each panel. The grafted quail cells were detected in the anterolateral portion of the endolymphatic system (es and ed; arrows in B-D) and in the anteromedial wall of the vestibule (arrows in E,F). The anterior crista was devoid of transplanted cells (arrowheads in F,G). (H) Schematic representation of the type 2 grafts (dT plus mT, dark and medium blue, respectively; *n*=6). (I-K) The grafted cells were detected in the utricule (u; I,J), entirely occupying its macula (mu; I-K). However, a part of the utricule was devoid of quail cells (arrowheads in I). A very small portion of the dorsal part of the macula sacculi showed QCPN-positive cells (ms in I,J; see also in K). The epithelium between the macula utriculi and macula sacculi was devoid of quail cells (red arrowheads in I,J). (L) Schematic representation of the type 3 grafts (dT, mT and vT; dark, medium and light blue, respectively; *n*=10). (M-P) Horizontal sections through rh4-ect type 3 chimeric embryos. Quail cells characterize the medial half of the anterior crista (ac; arrowheads in M,N) and a portion of the anterior vertical pouch (*a*-vp; M). In some cases, the borders of the grafted epithelium and the lateral crista were coincident (black arrowheads in O,P). The gap between the utricular and saccular maculae was QCPN positive (red arrowheads in O,P). The entire utricule was also QCPN positive (compare I,O). (Q,R) Three-dimensional diagrams of an E6 chimeric inner ear that summarize all these results. The three shades of blue representing the DV thirds are used. The sensory patches are represented by the red stippled areas. The horizontal section levels are indicated. A, anterior; C, caudal; D, dorsal; M, medial; P, posterior; R, rostral. AVG, acoustic-vestibular ganglion; bp, basilar papilla; cd, cochlear duct; hp, horizontal pouch; lc, lateral crista; mn, macula neglecta; ml, macula lagena; pc, posterior crista; *p*-vp, posterior vertical pouch; s, saccule. Scale bar: 36 µm.

anteromedial portion of the endolymphatic system, forming a DV band (Fig. 3B,C), similar and contiguous to the endolymphatic territory transplanted in rh4-ect type 1 experiments (Fig. 2B-D). In the vestibule, grafted cells were detected in a small area immediately medial to the insertion of the endolymphatic duct (not shown). Moreover, the macula sacculi contained quail cells in a small medial area (Fig. 3D,E). The QCPN-positive area invaded slightly into the proximal part of the basilar papilla in the cochlear duct, exclusively in its medial part (Fig. 3F,G).

The middle-third portion of the ectoderm opposite rh5 was then grafted in addition to the dorsal third (rh5-ect type 2; *n*=6; Fig. 3H). The *Fgf10*-positive macula sacculi showed QCPN-positive cells almost throughout (Fig. 3I,J), except in its dorsalmost portion (not shown; see Fig. 3I,J). A portion of the wall of the saccule was now also included in the transplanted area (Fig. 3I,J). The QCPN-labeled territory extended more laterally in the proximal cochlear duct, with the *Fgf10*-positive basilar papilla uniformly showing quail cells (Fig. 3K,L). In the proximal cochlear duct, the graft extended laterally far from the basilar papilla (Fig. 3K,L). The rest of the cochlear duct showed no grafted cells (Fig. 3S,T).

The entire cephalic ectoderm facing rh5 was then transplanted (rh5-ect type 3; Fig. 3M; *n*=11). In all cases, the type 3 graft extended rostrally towards the well-defined, *Fgf10*-positive anterior crista (Fig. 3N,O), therefore including the lateral wall of the anterior vertical pouch (Fig. 3N). Interestingly, the lateral half, but not the medial half (labeled in rh4 grafts), of the anterior crista was constituted by grafted rh5 cells (Fig. 3N,O). It is also significant that the entire horizontal pouch, the future lateral semicircular canal, was constituted by grafted cells (Fig. 3N). The *Fgf10*-positive lateral crista was now also included in the grafted epithelium (Fig. 3P). The macula sacculi was QCPN positive (complementing significantly the rh4-labeled medial portion), but not the macula utriculi (Fig. 3P,Q). In the proximal cochlear duct, the whole anterior half of its wall was QCPN immunopositive (Fig. 3R). Fig. 3S,T summarizes the

Development (2014) 141, 2302-2312 doi:10.1242/dev.101667

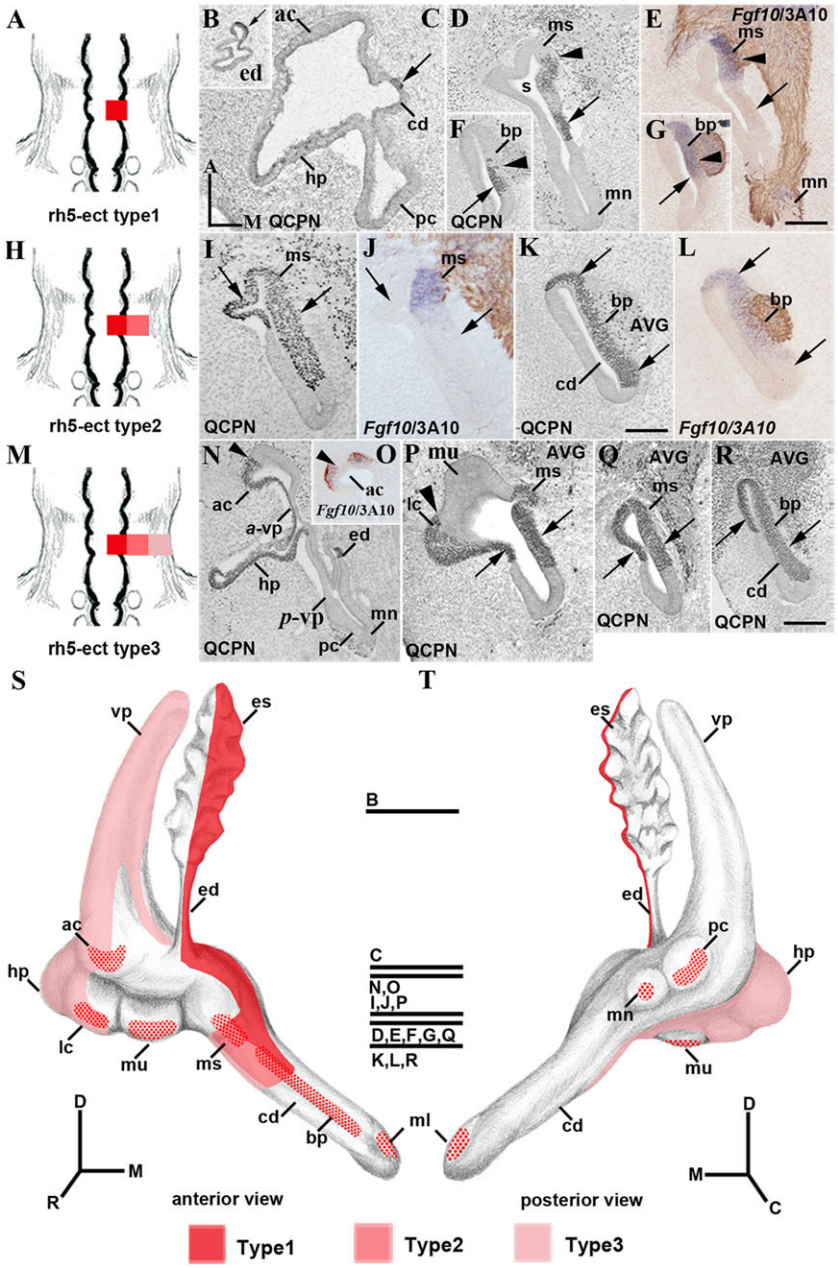

Fig. 3. Fate map of the otic placodal ectoderm facing rh5. (A) Schematic representation of the grafting results at the 10-somite stage of the rh5-ect type 1 experiment (dT; dark red; *n*=5). (B-G) Horizontal sections through an rh5-ect type 1 chimeric embryo at stage HH29 (E6). The quail cells were detected in the anteromedial portion of the endolymphatic system (arrows in B,C), extending ventrally in the medial wall of the vestibule (arrows in D,E) and the cochlear duct (arrows in F,G) to invade a small portion of both the saccular macula (arrowheads in D,E) and the proximal basilar papilla (arrowheads in F,G). (H) Schematic representation of the type 2 grafts (dT plus mT; dark and medium red, respectively; *n*=6). (I-L) Horizontal sections through an rh5-ect type 2 chimeric embryo. Quail cells were observed in the same portion of the endolymphatic system as in the rh5-ect type 1 (not shown; see B,C) and in a larger portion of the medial wall of the vestibule (arrows in I,J) and the proximal cochlear duct (arrows in K,L). The QCPN-positive cells were also detected in the macula sacculi (I,J) and the proximal basilar papilla (K,L). (M) Schematic representation of the grafting results of the rh5-ect type 3 experiment (dT, mT and vT; dark, medium and light red, respectively; *n*=11). (N-R) In horizontal sections through an rh5-ect type 3 chimera, the quail cells were detected in the endolymphatic system (N), the saccular macula (P,Q) and the proximal basilar papilla (R). The added portion in this type of transplant contributed to the entire horizontal pouch (N), the lateral crista (P), the lateral portion of the anterior vertical pouch (N), and the lateral half of the anterior crista (arrowheads in N,O). The arrowhead in P points to the common border of the graft and the lateral crista. (S,T) Three-dimensional diagrams of an E6 chimeric inner ear that summarize all these results. The three shades of red representing the DV thirds are used. Other abbreviations/labels as in Fig. 2. Scale bars: 45 μm in E; 40 μm in K; 36 μm in R.

respective distribution of cells derived from the three ectodermal sites examined (dT, mT and vT) opposite rh5.

The fate of the ectoderm opposite RhC

To determine the fate of the ectoderm facing prorhombomere C (RhC), which will divide into rh6 and rh7, we first focused on its rostral half, which would roughly correspond to future rh6 (Fig. 4). When the dorsal third of this ectoderm was transplanted (rh6-ect type 1; *n*=6; Fig. 4A), the quail-derived grafts formed a DV band located in the caudal aspect of the chimeric inner ear. QCPN-positive cells were detected in the caudal portion of the endolymphatic system (Fig. 4B). In the vestibule, quail cells were present in an epithelial area situated caudal to the insertion of the endolymphatic duct (Fig. 4C). In the cochlear duct, a narrow band formed by grafted cells contributed slightly to the caudalmost portion of the *Fgf10*-positive basilar papilla (Fig. 4D,E). A few scattered quail cells appeared dispersed a short distance outside of the grafted area (arrow in Fig. 4D, arrowhead in its inset). The macula lagena was located immediately caudal to the QCPN-immunostained area (Fig. 4F,G).

When the dorsal and middle thirds of the ectoderm opposite rostral RhC were grafted (rh6-ect type 2; *n*=10; Fig. 4H), a small portion of the posterior vertical pouch (*p*-vp) was labeled in addition to the caudomedial portion of the vestibule (Fig. 4I); the *p*-vp is directly implicated in the formation of the posterior semicircular canal. By contrast, the horizontal pouch was completely devoid of QCPN-positive cells (Fig. 4I). The ventral half of the macula neglecta was constituted by quail cells (Fig. 4K,L), whereas its dorsal half was devoid of QCPN-positive cells (Fig. 4Q). The rest of the vestibular sensory epithelia, including the posterior crista (Fig. 4I,J), did not contain quail cells in these experiments (Fig. 4I,K,L). In the distal cochlear duct, the quail transplant occupied a large portion of its wall (Fig. 4M,N). Thus, the distal basilar papilla and the entire macula lagena were constituted by grafted cells (Fig. 4M,N).

Development (2014) 141, 2302-2312 doi:10.1242/dev.101667

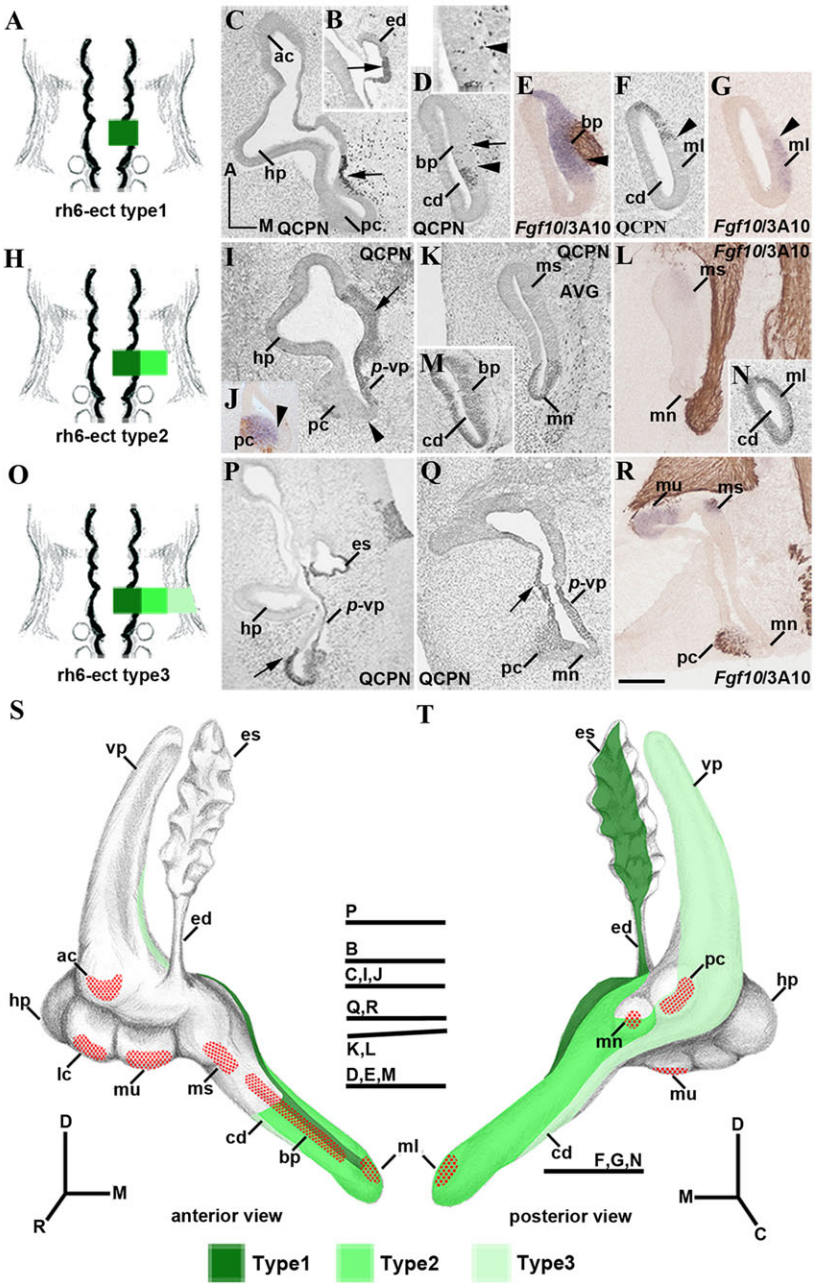

Fig. 4. Fate map of the otic placodal ectoderm facing the rostral half of the RhC (the future rh6). (A) Schematic representation of the grafting results at the 10-somite stage of the rh6-ect type 1 experiment (dT; dark green; *n*=6). (B-G) Horizontal sections through an rh6-ect type 1 chimeric embryo at stage HH29 (E6). The quail cells were detected in the posteromedial portion of the endolymphatic system (arrow in B) and in the medial wall of the vestibule, caudal to the insertion of the endolymphatic system (arrow in C). In the cochlear duct, the transplanted area formed a small DV band invading slightly into the distal basilar papilla (arrowheads in D,E). Some scattered quail cells were found outside the graft (arrow in D; arrowhead in the inset in D). The graft delimited the macula lagena (arrowheads in F,G). (H) Schematic representation of the grafting results (dT plus mT; dark and medium green, respectively; *n*=10). (I-N) Grafted ectoderm was detected additionally in the posterior vertical pouch (I). The posterior crista showed no quail cells (arrowheads in I,J). The ventral part of the macula neglecta (K), as well as the entire extent of both the distal basilar papilla (M) and the macula lagena (N), were QCPN positive. The whole distal cochlear duct epithelium is constituted by quail cells (M,N). (O) Schematic representation of the type 3 grafts (dT, mT and vT; dark, medium, and light green, respectively; *n*=11). (P-R) Note the presence of quail cells in the posterior part of the vertical pouch (arrows in P,Q) and the entire *Fgf10*-positive posterior crista (Q,R), whereas the dorsal portion of the macula neglecta remained QCPN negative (Q). (S,T) The three shades of green represent the grafted third derivatives (dT, mT and vT) for the placodal ectoderm facing the rostral half of the RhC (r6). Abbreviations/labels as in Fig. 2. Scale bar: 41 μm.

The entire ectoderm facing the rostral half of the RhC was then grafted (rh6-ect type 3; *n*=11; Fig. 4O). This kind of transplantation confirmed that the ventral third of the local ectoderm (vT) will contribute to the posterior portion of the vertical pouch (*p*-vp in Fig. 4P,Q). The posterior crista was completely included in the grafted territory as well (Fig. 4Q,R). The dorsal part of the macula neglecta was devoid of grafted cells (Fig. 4Q), although some quail cells were observed in its ventral portion (Fig. 4K). Fig. 4S,T summarize the distribution of cells resulting from the three ectoderm domains (dT, mT and vT) examined opposite the prospective rh6.

Finally, we considered the ectoderm grafts facing the caudal half of the RhC (prospective rh7). When the dorsal third of this ectoderm was transplanted (rh7-ect type 1; *n*=6; Fig. 5A), the quail grafts were found exclusively in a very small caudolateral portion of the endolymphatic apparatus (not shown; see Fig. 5B). Chimeric embryos with rh7-ect type 2 grafts (*n*=6; Fig. 5A) showed additional labeling in the dorsal half of the macula neglecta (Fig. 5E,F), whereas its ventral half was devoid of QCPN-positive cells (Fig. 5G,H; see also rh6-ect type 2, Fig. 4K,L). The grafted middle-third territory was also observed in the vestibule (Fig. 5C), but far from the posterior crista (Fig. 5C,D). In addition to the rh7-ect type 2 results, rh7-ect type 3 experiments showed labeling of a small portion of the caudal vertical pouch (*n*=9; not shown; see Fig. 5I,J). Fig. 5I,J summarize all these results in a stage E6 inner ear.

DiI labeling experiments

In order to better define the borders of the otic placode within our 4×3 experimental grid, DiI labeling experiments were performed at the 10-somite stage and analyzed at the otic cup stage, determining whether they fell inside or outside of the presumptive otic vesicle. DiI crystals were placed in the peripheral area of the ectoderm strips, the central part of which included the otic placode. We observed that a narrow peripheral band of the analyzed ectoderm does not

Development (2014) 141, 2302-2312 doi:10.1242/dev.101667

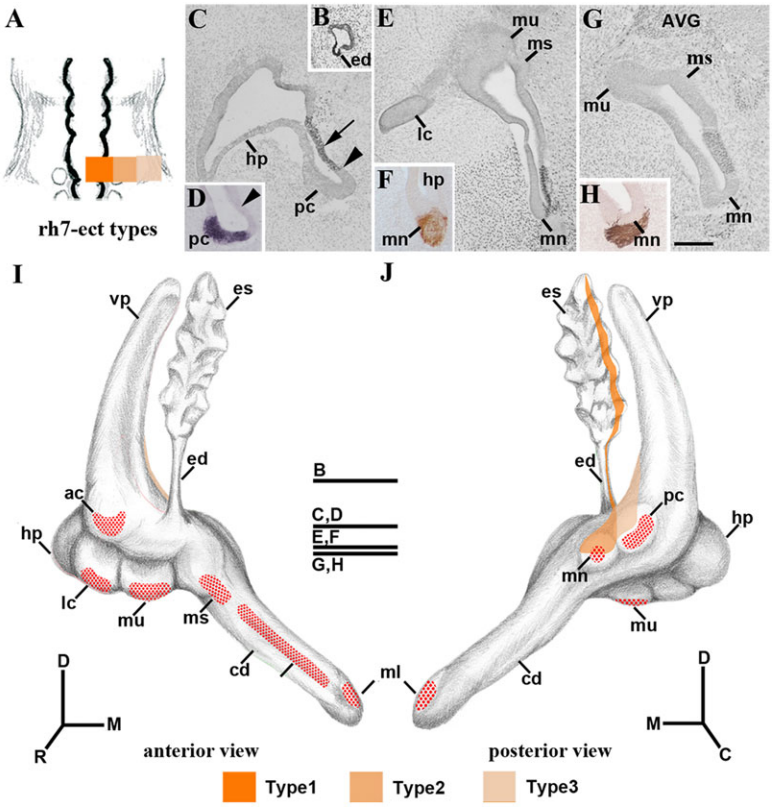

Fig. 5. Fate map of the otic placodal ectoderm facing the caudal half of the RhC (the future rh7). (A) Schematic representation of the grafting experimental design at the 10-somite stage. (B-H) Horizontal sections through an rh7-ect type 2 chimeric embryo at stage HH29 (E6; *n*=6). The quail cells were detected in the endolymphatic system (B) and in the caudal aspect of the chimeric inner ear (arrow in C). The dorsal half of the innervated macula neglecta (E,F), but not its ventral half (G,H), exhibit QCPN-positive cells. The posterior crista was devoid of quail cells (arrowheads in C,D). (I,J) Three-dimensional diagrams of an E6 chimeric inner ear summarizing the fate of the three DV thirds considered for the placodal ectoderm facing the caudal half of the RhC (dT, mT and vT; dark, medium and light orange, respectively). Abbreviations/labels as in Fig. 2. Scale bar: 35 µm.

contribute to chick inner ear formation (Fig. 6). These results agreed with the fate map reported by Brigande et al. (2000a).

Fate map

Fig. 7 summarizes the fate of the 12 ectoderm domains that contribute to the otic placode (Fig. 7A), as read out in the inner ear at E6 (Fig. 7B), using the same color-code to map each set of experiments. Regarding the sensory patches of the developing inner ear, our preparations revealed that: (1) the macula utriculi and a part of the anterior crista, as well as a small portion of the macula sacculi and lateral crista, originated from the ectoderm facing rh4; (2) the rest of the macula sacculi and lateral crista, as well as the complementary portion of the anterior crista, in addition to the proximal part of the basilar papilla, originated from the ectoderm opposite rh5; (3) the entire macula lagena and posterior crista, as well as one half of the macula neglecta, and the distal basilar papilla, came from the ectoderm facing the rostral RhC (presumptive rh6); and (4) the remaining half of the macula neglecta originated opposite the caudal RhC (presumptive rh7). The origin of the non-sensory elements was also determined (Fig. 8).

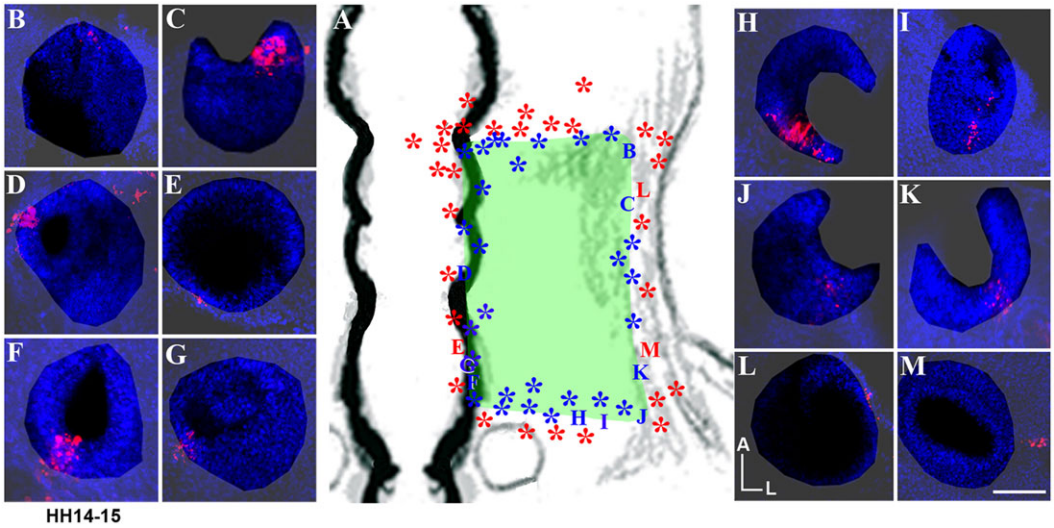

Fig. 6. Delimitation of the otic placode border (prospective otic pore) at the 10-somite stage. (A) Schematic representation of the otic placode in which the locations of individually inserted DiI crystals are indicated. (B-M) Images at HH14-15 stage showing the DiI-labeled cells in the otic cup epithelium (B-D,G-K, indicated in blue in A) or in the ectoderm outside the otic anlagen (E,L,M, indicated in red in A). The blue and red asterisks in A represent the markings falling inside and outside the otic epithelium (green area), respectively. A, anterior; L, lateral. Scale bar: 60 µm.

Development (2014) 141, 2302-2312 doi:10.1242/dev.101667

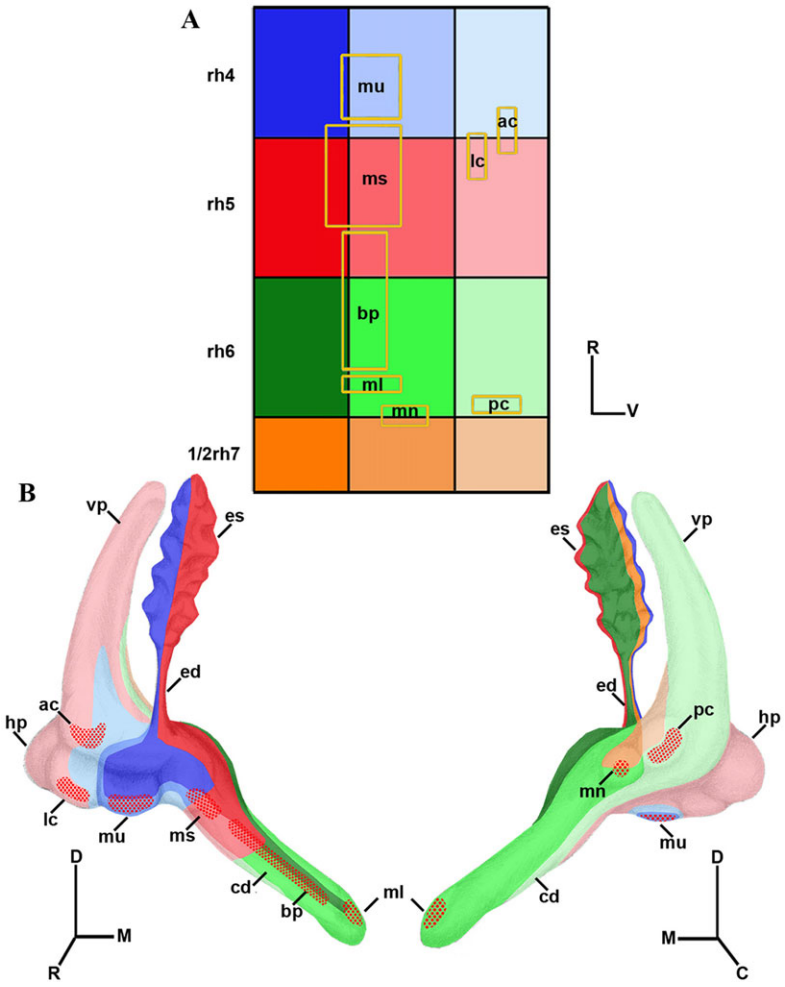

Fig. 7. Fate map of the chick otic placode. (A) Schematic representation of the fate map of the avian otic placode at the 10-somite stage, focusing on the relative positions of the presumptive sensory and non-sensory elements of the inner ear. The distribution of the 12 Cartesian parts considered within the otic placodal operation field is indicated. The same color-code as used in previous figures is maintained. Dorsal is to the left and rostral is up. The neuromeric subdivisions of the hindbrain (rh) are also indicated. (B) Three-dimensional diagrams of an E6 chimeric inner ear summarizing the fate of all the portions considered in this study. The sensory patches are represented by the red stippled areas. ac, anterior crista; bp, basilar papilla; cd, cochlear duct; ed, endolymphatic duct; es, endolymphatic sac; hp, horizontal pouch; lc, lateral crista; ml, macula lagena; mn, macula neglecta; ms, macula sacculi; mu, macula utriculi; pc, posterior crista; vp, vertical pouch. C, caudal; D, dorsal; M, medial; R, rostral; V, ventral.

Remarkably, the endolymphatic system clearly derives from the dorsalmost part of the otic placode (Fig. 8).

To confirm the fate map obtained from the 12 grafting experiments presented above, three new kinds of graft have now been performed (supplementary material Fig. S1). (1) Similar portions (types 1-3) of two contiguous rhombomeres were grafted and the fates analyzed (n=25). (2) The dorsal half of the ectoderm facing a rhombomere was also grafted and the fate was analyzed (n=12). (3) To remove any possible doubts, we performed additional experiments but now cutting the cephalic ectoderm along a line perpendicular to the neural tube passing through the middle of a rhombomere. Graft sizes equivalent to two or three contiguous rhombomeres were also employed (n=17). Out of this additional round of grafting experiments new chimeric cases were analyzed (n=10; supplementary material Figs S2-S4). In all these new grafts, the location of the graft borders was absolutely coincident with the fate mapping study obtained above, confirming once again the illustrated fate map showing the location of sensory and non-sensory organs within a Cartesian coordinate positional system.

DISCUSSION

Specification of the trigeminal, otic and epibranchial placodes

The chick otic placode is morphologically first perceptible around the 10-somite stage on both sides of the hindbrain. Previous early fate mapping studies, which involved placing the fluorescent dyes DiI and/or DiO in the chick epiblast (Streit, 2002), did not investigate the 10-somite stage (the subject of this work), and focused instead on a preceding developmental period, namely the head process and 4-somite stage (HH8). At stage HH8, the otic placode precursors are scattered and intermingled with those of other nearby embryonic tissues, in particular the trigeminal placode (see also Stevenson et al., 2012; stage HH7). Extensive cell movements bring otic precursors gradually to convergence within a defined otic placode, and are then entirely isolated, especially with respect to the trigeminal placode. This result has been confirmed in *Xenopus*, zebrafish and chick embryos (McCarroll et al., 2012; Stevenson et al., 2012). The trigeminal *Otx2*-positive and the otic *Gbx2*-positive domains showed reduced overlap at stage HH7 and were exclusive soon thereafter, strongly suggesting the existence of a repressor-modulated molecular mechanism for the segregation of sensory progenitors into different placodal fates (Stevenson et al., 2012; see also Hidalgo-Sánchez et al., 2000). Our studies with DiI labeling at the 10-somite stage rule out any contribution of the cephalic ectoderm facing r3 to the otic placode, and also make clear the contribution of ectoderm facing r4 to the future inner ear rudiment. Therefore, results of the present work and those of Stevenson et al. (2012) disagree with the fate map reported for the ophthalmic and maxillomandibular trigeminal placodes in the chick embryo (Xu et al., 2008), which concludes that cells labeled at the cephalic ectoderm at the level of rh3-4, even at the 15/16-somite stage, will be incorporated into the otic vesicle (Xu et al., 2008).

Development (2014) 141, 2302-2312 doi:10.1242/dev.101667

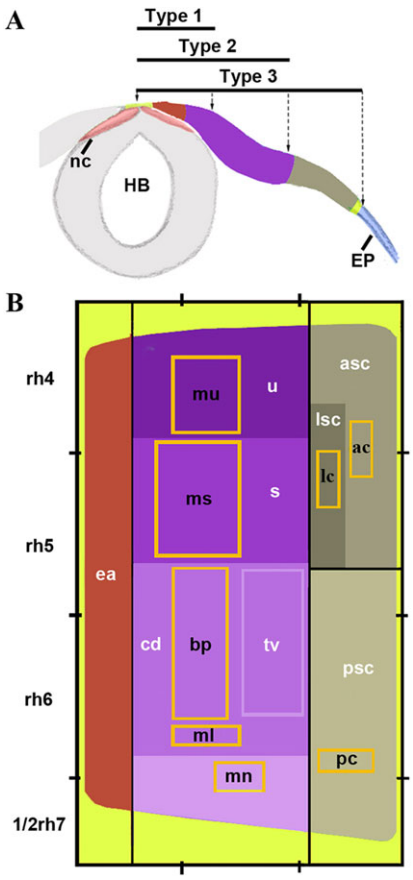

Fig. 8. Fate map of the chick otic placode. (A) Transverse section at the level of the otic placode showing the subdivision of the otic-epibranchial field into stripe-like longitudinal domains arranged dorsoventrally. (B) Schematic representation of the fate map of the avian otic placode at the 10-somite stage showing the origin of the sensory and non-sensory elements of the chick inner ear with respect to the adjacent rhombomeres and the stripe-like longitudinal domains. The non-otic or extraplacodal portion is indicated in yellow. asc, anterior semicircular canal; EP, epidermis; ea, endolymphatic apparatus; HB, hindbrain; lsc; lateral semicircular canal; nc, neural crest; psc, posterior semicircular canal; s, saccule; tv, tegmentum vasculosum; u, utricle. Other abbreviations as in Fig. 7.

It is possible (as suggested by results from this work) that some reported fate maps in the chick overestimate cell mixing between the trigeminal and otic placodes at the 10-somite stage. A similar conclusion was reached recently for *Xenopus* embryos using both grafts and DiI/DiO labeling experiments for studies of the origin and segregation of cranial placodes (Pieper et al., 2011; see also Schlosser, 2010; Stevenson et al., 2012). The fact that the epibranchial placode precursors are also restricted along the AP axis of the *Pax2*-positive ectodermal domain at early stages of somitogenesis strongly supports this contention (McCarroll et al., 2012).

DV and AP patterning of the otic placode

It is well known that the inner ear and the otic and epibranchial placodes arise from a common progenitor domain, termed the posterior placodal field (Ladher et al., 2010), which is *Pax2* positive (Baker and Bronner-Fraser, 2000; McCarroll et al., 2012; Streit, 2002). FGF signaling from the underlying segmented paraxial mesoderm causes its early induction in the competent ectoderm (reviewed by Ohyama et al., 2007; Schimmang, 2007; see also Padanad et al., 2012; Yang et al., 2013). Thus, early patterning of the head mesoderm, governed by a dynamic combination of extrinsic cues (Bothe et al., 2011), plays a pivotal role in early otic-epibranchial induction, separating this primordium from other ectodermal derivatives (Baker and Bronner-Fraser, 2001). Once this large otic-epibranchial field has been specified in the cephalic ectoderm, an elaborate network of additional signals is involved in further patterning processes within it.

Regarding the developing inner ear, our data suggest a DV specification of the otic-epibranchial placodal field into stripe-like longitudinal domains with distinct fates; this pattern might depend on a DV gradient of a morphogen that diffuses from the dorsal midline of the embryo. It is known that canonical WNT signaling from the dorsal neural tube and/or dorsal ectoderm (Riccomagno et al., 2005) acts after the induction of the posterior placodal area by FGF (Bok et al., 2007; Ladher et al., 2010). This molecular mechanism is directly involved in the placodal versus epibranchial-epidermis fate decisions, conferring otic identity upon the medial (dorsal) part of the *Pax2*-expressing domain (Ohyama et al., 2006). Attenuation of mitogenic FGF activity and activation of the differentiation-inducing WNT signaling pathway leads to expanded otic commitment and local repression of the epibranchial fate (McCarroll et al., 2012; Ohyama et al., 2006). In addition, the BMP signaling pathways are also relevant in early regionalization of the otic-epibranchial placodal field (Abelló et al., 2010; Begbie et al., 1999; Holzschuh et al., 2005). Hence, the spatiotemporally orchestrated actions of several signaling pathways possibly determine the final cell fates of otic progenitors, at least as regards their organization into superposed longitudinal stripe-like domains with distinct fates.

According to the present data, the cells of the dorsalmost band, probably influenced by higher concentrations of dorsal morphogens, will give rise to the endolymphatic system, whereas the ventralmost band, located far from the hypothetical dorsal morphogen source, will develop into the cristae and their associated semicircular canals. Between these two bands, a third domain will give rise to most of the maculae plus the macular-derived basilar papilla, accompanied by their attached non-sensory epithelia (Fig. 8). The fact that *Bmp7* and *Lmx1b* expression patterns and Wnt/β-catenin activity characterize longitudinal territories located in the dorsal part of the otic placode (8- to 9-somite stage) strongly supports this stripe-like DV patterning model (Abelló et al., 2010; Riccomagno et al., 2005). A fourth AP band, located ventral to the otic placode, would represent the domain from which the epibranchial placode arises (Ladher et al., 2010). This fourth band is possibly specified by the same gradient mechanism.

Other gradient effects oriented orthogonally to the DV mechanism must control the specification of AP differences within the otic placode. Various authors have likewise postulated the existence of driving forces that govern the patterning of the otic placode along its AP axis (Abelló et al., 2007; Bok et al., 2007; Léger and Brand, 2002). A relevant transverse organizing center might be established rostrally. Interestingly, chick embryos show a narrow band of *Fgf8* expression that appears at the border of the *Gbx2*-positive otic placode with the *Otx2*-positive trigeminal placode (Hidalgo-Sánchez et al., 2000; for comments on *Otx2*/*Gbx2* mutual repression, see Stevenson et al., 2012). Similarly, as is widely accepted for the isthmic organizer, the confrontation of antagonistic *Otx2*-expressing and *Gbx2*-expressing epithelial domains might induce the creation of an intercalated otic/trigeminal organizing center that expresses *Fgf8* and releases FGF8 as a diffusing morphogen (Hidalgo-Sánchez et al., 2005). The gradient-governed interaction of DV and AP organizing centers would establish a Cartesian coordinate positional system for differential molecular signaling in the otic placodal field (Meinhardt, 2008).

Development (2014) 141, 2302-2312 doi:10.1242/dev.101667

However, we cannot rule out other possibilities that have been suggested for DV and AP patterning, in particular the relevance of Shh and retinoic acid signals (Bok et al., 2007, 2011; Brown and Epstein, 2011; Hammond and Whitfield, 2011; Riccomagno et al., 2005; Wu et al., 1998). Restricted spot-like signaling centers from the segmented hindbrain, or even from the pharyngeal endoderm and subjacent mesoderm, might also be involved directly or indirectly in otic placode specification, representing potential sources of additional differential AP signals (Abelló et al., 2010; Alsina et al., 2009; Baker et al., 2008; Begbie et al., 1999; Chen and Streit, 2013; Graham, 2008; Grocott et al., 2012; Ladher et al., 2010; Lleras-Forero and Streit, 2012; McCabe and Bronner-Fraser, 2009; Schlosser, 2006, 2010; Schneider-Maunoury and Pujades, 2007; Whitfield and Hammond, 2007).

Conclusions

We visualize the otic placode as a two-dimensional field organized along the AP and DV axes, which are probably defined by early gradient-distributed inductive and positional signals, later complemented by various point-like signaling effects. By the otic cup stage, additional intrinsic and extrinsic signaling pathways, secondary to the preliminary mechanisms acting at the placodal stage, will trigger and modulate the multi-step (combined) mechanism for the specification of distinct sensory and non-sensory patches within the developing otic rudiment (reviewed by Bok et al., 2007). Thus, subsequent morphogenetic phenomena – for instance the differential rate of proliferation and cell death in the posterior placodal field (Washausen et al., 2005) – would result in the creation of the three-dimensional structure of the otic vesicle around a fluid-filled cavity.

The understanding of otic morphogenetic events now allows us to employ in any morphological description either two-dimensional topological Cartesian coordinates derived from the placodal stage or polar coordinates corresponding to the cup or vesicular stages. We believe that such a conversion would reduce possible interpretational mistakes when different developmental stages are being compared, or when the topology of a signaling effect is unclear. In this sense, current understanding of the fate of the primary axes of the otic rudiment from the otic cup stage onwards should be revised, particularly in the case of the DV axis.

This fate mapping study has systemized for the first time otic differential fates in a flat Cartesian positional model of intercrossing longitudinal epithelial stripes and transverse paraneuromeric domains. Distinct otic epithelial compartments, presumptively created by position-dependent activation or repression of specific genes already at placodal stages, could define subsequent borders of lineage restriction, gene expression and fate within the developing otic anlage. These regional DV and AP molecular identities, plus theoretically predicted antagonistic local activation and long-range inhibition phenomena (Meinhardt, 2008), could culminate in the species-specific distribution of sensory epithelia in the membranous labyrinth (Fekete, 1996; Fekete and Wu, 2002). Note that transient developmental boundaries produced between initial compartments may generate new signaling mechanisms (Hidalgo-Sánchez et al., 2005; Meinhardt, 2008). At the otic cup stage, or even later, new inductive or inhibitory signals generated in the otic epithelium itself (such as sources of FGFs, BMPs, WNTs and retinoic acid) are apparently decisive for the final modeling of the inner ear in amniotes (Romand et al., 2006; Sánchez-Guardado et al., 2009, 2013; Sienknecht and Fekete, 2009; Whitfield and Hammond, 2007). Our results are therefore consistent with an open-ended compartmental model (Fekete, 1996; Brigande et al., 2000b; Fekete and Wu, 2002).

In summary, this fate mapping study promises to aid in the quest to understand how diverse molecular agents control asymmetric expression patterns of various regulatory genes, with important morphogenetic consequences in differential growth, differentiation and histogenesis. This experimental fate map of the chick otic placode also helps to anchor the plethora of existing descriptive and experimental data about otic epithelium patterning in a new developmental context. Moreover, the placodal otic fate map allows developmental biologists to design innovative functional studies to examine the molecular mechanisms involved in the specification of all the vestibular and auditory structures in the developing vertebrate inner ear.

MATERIALS AND METHODS

Processing of the tissue

Fertilized White Leghorn chick (*Gallus gallus*) and Japanese quail (*Coturnix coturnix japonica*) eggs were incubated in a humidified atmosphere at 38±1°C. Chimeric embryos were fixed and processed for cryostat sectioning as previously described (Sánchez-Guardado et al., 2009).

Grafting experiments

Chick and quail embryos were used to obtain chimeras by exchanging specific portions of the cephalic ectoderm adjacent to the hindbrain (Vaage, 1969) at stage HH10 (exactly 10 somites; Hamburger and Hamilton, 1992) in unilateral homotopic and isochronic transplants (Le Douarin, 1969). The constrictions between rhombomeres (or prorhombomeres) served as landmarks. A grid inserted into one ocular of the operating microscope helped to define the three DV divisions of the otic placode. In all cases, the chick embryo was the host and the quail embryo the donor. The microsurgical procedure *in ovo* was that described in detail by Alvarado-Mallart and Sotelo (1984). A small portion of the alar plate of the neural tube and the intervening mesenchyme was also jointly transplanted to obtain a more solid graft and ensure the integration of the grafts in the host (Fig. 1). After transplantation, the host eggs were closed with Parafilm, sealed with paraffin, and kept at 38±1°C. The resulting chimeric embryos were analyzed at 6-8 days of incubation (stages HH29-34), when major morphogenetic changes had already taken place (Bissonnette and Fekete, 1996; Sánchez-Guardado et al., 2013).

Note on surgery

The grafts of quail tissue were perfectly integrated in the chick host in less than 3 hours. After this period, the quail graft always occupied exactly the holes made in the host chick embryo in such a way that it was not possible to identify without specific labeling the donor/host interface (Hidalgo-Sánchez et al., 1999). Therefore, since the experimental injury healed very well, any possible alteration caused by the wound is obviated.

In situ hybridization and immunohistochemistry staining

In situ hybridization was performed on cryosections as described by Sánchez-Guardado et al. (2011). The chick *Fgf10* subclone used in this study is described elsewhere (Sánchez-Guardado et al., 2013). To visualize the grafted cells, the QCPN monoclonal mouse antibody (Developmental Studies Hybridoma Bank; 1/100) was used, which specifically identifies quail cells among unstained chick tissues (for the procedure, see Hidalgo-Sánchez et al., 1999). Immunoreaction with the 3A10 antibody [Developmental Studies Hybridoma Bank (DSHB), mouse, monoclonal, #3A10, 1:40] is a useful tool to label the axons of the acoustic-vestibular ganglion neurons and to aid in the identification of presumptive sensory epithelia (for the procedure, see Sánchez-Guardado et al., 2013).

DiI injections

Small lipophilic dye (DiI) crystals were selectively placed *in ovo* at the predicted border of the otic placodal ectoderm, using the tip of a pulled glass micropipette (Bell et al., 2008). These experimental embryos were fixed at the otic cup stage (HH14-15; just prior to the closure of the otic pore) in 4%

formaldehyde in PBS for 6 h, washed in PBS, and prepared for cryosectioning. The histological location of the DiI-labeled cells was then imaged using epifluorescence. Only cases in which the placement of the DiI crystal was restricted to a small group of cells were analyzed.

Acknowledgements
We are grateful to Rosa-Magda Alvarado-Mallart for inspiring us to carry out this work, which is dedicated to her memory.

Competing interests
The authors declare no competing financial interests.

Author contributions
M.H.-S., L.O.S.-G. and L.P. designed experiments, analyzed data and wrote the manuscript. L.O.S.-G. and M.H.-S. performed experiments.

Funding
This work was supported by the Spanish Ministry of Science [BFU2010-19461 to M.H.-S., BFU2005-09378-C02-01 and BFU2008-04156 to L.P.]; the SENECA Foundation [04548/GERM/06-10891 to L.P.]; and a Junta-de-Extremadura predoctoral studentship [PRE/08031 to L.O.S.-G.].

Supplementary material
Supplementary material available online at
http://dev.biologists.org/lookup/suppl/doi:10.1242/dev.101667/-/DC1

References
Abelló, G., Khatri, S., Giráldez, F. and Alsina, B. (2007). Early regionalization of the otic placode and its regulation by the Notch signaling pathway. *Mech. Dev.* **124**, 631-645.
Abelló, G., Khatri, S., Radosevic, M., Scotting, P. J., Giráldez, F. and Alsina, B. (2010). Independent regulation of Sox3 and Lmx1b by FGF and BMP signaling influences the neurogenic and non-neurogenic domains in the chick otic placode. *Dev. Biol.* **339**, 166-178.
Alsina, B., Giraldez, F. and Pujades, C. (2009). Patterning and cell fate in ear development. *Int. J. Dev. Biol.* **53**, 1503-1513.
Alvarado-Mallart, R.-M. and Sotelo, C. (1984). Homotopic and heterotopic transplantations of quail tectal primordia in chick embryos: organization of the retinotectal projections in the chimeric embryos. *Dev. Biol.* **103**, 378-398.
Baker, C. V. H. and Bronner-Fraser, M. (2000). Establishing neuronal identity in vertebrate neurogenic placodes. *Development* **127**, 3045-3056.
Baker, C. V. H. and Bronner-Fraser, M. (2001). Vertebrate cranial placodes I. Embryonic induction. *Dev. Biol.* **232**, 1-61.
Baker, C. V. H., O'Neill, P. and McCole, R. B. (2008). Lateral line, otic and epibranchial placodes: developmental and evolutionary links? *J. Exp. Zool. B Mol. Dev. Evol.* **310B**, 370-383.
Begbie, J., Brunet, J. F., Rubenstein, J. L. and Graham, A. (1999). Induction of the epibranchial placodes. *Development* **126**, 895-902.
Bell, D., Streit, A., Gorospe, I., Varela-Nieto, I., Alsina, B. and Giraldez, F. (2008). Spatial and temporal segregation of auditory and vestibular neurons in the otic placode. *Dev. Biol.* **322**, 109-120.
Bissonnette, J. P. and Fekete, D. M. (1996). Standard atlas of the gross anatomy of the developing inner ear of the chicken. *J. Comp. Neurol.* **368**, 620-630.
Bok, J., Chang, W. and Wu, D. K. (2007). Patterning and morphogenesis of the vertebrate inner ear. *Int. J. Dev. Biol.* **51**, 521-533.
Bok, J., Raft, S., Kong, K.-A., Koo, S. K., Dräger, U. C. and Wu, D. K. (2011). Transient retinoic acid signaling confers anterior-posterior polarity to the inner ear. *Proc. Natl. Acad. Sci. U.S.A.* **108**, 161-166.
Bothe, I., Tenin, G., Oseni, A. and Dietrich, S. (2011). Dynamic control of head mesoderm patterning. *Development* **138**, 2807-2821.
Brigande, J. V., Iten, L. E. and Fekete, D. M. (2000a). A fate map of chick otic cup closure reveals lineage boundaries in the dorsal otocyst. *Dev. Biol.* **227**, 256-270.
Brigande, J. V., Kiernan, A. E., Gao, X., Iten, L. E. and Fekete, D. M. (2000b). Molecular genetics of pattern formation in the inner ear: do compartment boundaries play a role? *Proc. Natl. Acad. Sci. U.S.A.* **97**, 11700-11706.
Brown, A. S. and Epstein, D. J. (2011). Otic ablation of smoothened reveals direct and indirect requirements for Hedgehog signaling in inner ear development. *Development* **138**, 3967-3976.
Chen, J. and Streit, A. (2013). Induction of the inner ear: stepwise specification of otic fate from multipotent progenitors. *Hear. Res.* **297**, 3-12.
Dahmann, C. and Basler, K. (1999). Compartment boundaries: at the edge of development. *Trends Genet.* **15**, 320-326.
Fekete, D. M. (1996). Cell fate specification in the inner ear. *Curr. Opin. Neurobiol.* **6**, 533-541.
Fekete, D. M. and Wu, D. K. (2002). Revisiting cell fate specification in the inner ear. *Curr. Opin. Neurobiol.* **12**, 35-42.
Graham, A. (2008). Deconstructing the pharyngeal metamere. *J. Exp. Zool. B Mol. Dev. Evol.* **310B**, 336-344.
Grocott, T., Tambalo, M. and Streit, A. (2012). The peripheral sensory nervous system in the vertebrate head: a gene regulatory perspective. *Dev. Biol.* **370**, 3-23.
Hamburger, V. and Hamilton, H. L. (1992). A series of normal stages in the development of the chick embryo. *Dev. Dyn.* **195**, 231-272.
Hammond, K. L. and Whitfield, T. T. (2011). Fgf and Hh signalling act on a symmetrical pre-pattern to specify anterior and posterior identity in the zebrafish otic placode and vesicle. *Development* **138**, 3977-3987.
Hidalgo-Sánchez, M., Simeone, A. and Alvarado-Mallart, R. M. (1999). Fgf8 and Gbx2 induction concomitant with Otx2 repression is correlated with midbrain-hindbrain fate of caudal prosencephalon. *Development* **126**, 3191-3203.
Hidalgo-Sánchez, M., Alvarado-Mallart, R.-M. and Alvarez, I. S. (2000). Pax2, Otx2, Gbx2 and Fgf8 expression in early otic vesicle development. *Mech. Dev.* **95**, 225-229.
Hidalgo-Sánchez, M., Millet, S., Bloch-Gallego, E. and Alvarado-Mallart, R.-M. (2005). Specification of the meso-isthmo-cerebellar region: the Otx2/Gbx2 boundary. *Brain Res. Brain Res. Rev.* **49**, 134-149.
Holzschuh, J., Wada, N., Wada, C., Schaffer, A., Javidan, Y., Tallafuss, A., Bally-Cuif, L. and Schilling, T. F. (2005). Requirements for endoderm and BMP signaling in sensory neurogenesis in zebrafish. *Development* **132**, 3731-3742.
Kil, S.-H. and Collazo, A. (2001). Origins of inner ear sensory organs revealed by fate map and time-lapse analyses. *Dev. Biol.* **233**, 365-379.
Kil, S.-H. and Collazo, A. (2002). A review of inner ear fate maps and cell lineage studies. *J. Neurobiol.* **53**, 129-142.
Kozlowski, D. J., Murakami, T., Ho, R. K. and Weinberg, E. S. (1997). Regional cell movement and tissue patterning in the zebrafish embryo revealed by fate mapping with caged fluorescein. *Biochem. Cell Biol.* **75**, 551-562.
Ladher, R. K., O'Neill, P. and Begbie, J. (2010). From shared lineage to distinct functions: the development of the inner ear and epibranchial placodes. *Development* **137**, 1777-1785.
Lang, H. and Fekete, D. M. (2001). Lineage analysis in the chicken inner ear shows differences in clonal dispersion for epithelial, neuronal, and mesenchymal cells. *Dev. Biol.* **234**, 120-137.
Le Douarin, N. M. (1969). Details of the interphase nucleus in Japanese quail (Coturnix coturnix japonica). *Bull. Biol. Fr. Belg.* **103**, 435-452.
Léger, S. and Brand, M. (2002). Fgf8 and Fgf3 are required for zebrafish ear placode induction, maintenance and inner ear patterning. *Mech. Dev.* **119**, 91-108.
Li, C. W., Van De Water, T. R. and Ruben, R. J. (1978). The fate mapping of the eleventh and twelfth day mouse otocyst: an in vitro study of the sites of origin of the embryonic inner ear sensory structures. *J. Morphol.* **157**, 249-267.
Lleras-Forero, L. and Streit, A. (2012). Development of the sensory nervous system in the vertebrate head: the importance of being on time. *Curr. Opin. Genet. Dev.* **22**, 315-322.
McCabe, K. L. and Bronner-Fraser, M. (2009). Molecular and tissue interactions governing induction of cranial ectodermal placodes. *Dev. Biol.* **332**, 189-195.
McCarroll, M. N., Lewis, Z. R., Culbertson, M. D., Martin, B. L., Kimelman, D. and Nechiporuk, A. V. (2012). Graded levels of Pax2a and Pax8 regulate cell differentiation during sensory placode formation. *Development* **139**, 2740-2750.
Meinhardt, H. (2008). Models of biological pattern formation: from elementary steps to the organization of embryonic axes. *Curr. Top. Dev. Biol.* **81**, 1-63.
Ohyama, T., Mohamed, O. A., Taketo, M. M., Dufort, D. and Groves, A. K. (2006). Wnt signals mediate a fate decision between otic placode and epidermis. *Development* **133**, 865-875.
Ohyama, T., Groves, A. K. and Martin, K. (2007). The first steps towards hearing: mechanisms of otic placode induction. *Int. J. Dev. Biol.* **51**, 463-472.
Padanad, M. S., Bhat, N., Guo, B. and Riley, B. B. (2012). Conditions that influence the response to Fgf during otic placode induction. *Dev. Biol.* **364**, 1-10.
Pieper, M., Eagleson, G. W., Wosniok, W. and Schlosser, G. (2011). Origin and segregation of cranial placodes in Xenopus laevis. *Dev. Biol.* **360**, 257-275.
Riccomagno, M. M., Takada, S. and Epstein, D. J. (2005). Wnt-dependent regulation of inner ear morphogenesis is balanced by the opposing and supporting roles of Shh. *Genes Dev.* **19**, 1612-1623.
Romand, R., Dollé, P. and Hashino, E. (2006). Retinoid signaling in inner ear development. *J. Neurobiol.* **66**, 687-704.
Sánchez-Guardado, L. O., Ferran, J. L., Mijares, J., Puelles, L., Rodríguez-Gallardo, L. and Hidalgo-Sánchez, M. (2009). Raldh3 gene expression pattern in the developing chicken inner ear. *J. Comp. Neurol.* **514**, 49-65.
Sánchez-Guardado, L. O., Ferran, J. L., Rodríguez-Gallardo, L., Puelles, L. and Hidalgo-Sánchez, M. (2011). Meis gene expression patterns in the developing chicken inner ear. *J. Comp. Neurol.* **519**, 125-147.
Sánchez-Guardado, L. O., Puelles, L. and Hidalgo-Sánchez, M. (2013). Fgf10 expression patterns in the developing chick inner ear. *J. Comp. Neurol.* **521**, 1136-1164.
Satoh, T. and Fekete, D. M. (2005). Clonal analysis of the relationships between mechanosensory cells and the neurons that innervate them in the chicken ear. *Development* **132**, 1687-1697.

Schimmang, T. (2007). Expression and functions of FGF ligands during early otic development. *Int. J. Dev. Biol.* **51**, 473-481.
Schlosser, G. (2006). Induction and specification of cranial placodes. *Dev. Biol.* **294**, 303-351.
Schlosser, G. (2010). Making senses development of vertebrate cranial placodes. *Int. Rev. Cell. Mol. Biol.* **283**, 129-234.
Schneider-Maunoury, S. and Pujades, C. (2007). Hindbrain signals in otic regionalization: walk on the wild side. *Int. J. Dev. Biol.* **51**, 495-506.
Sienknecht, U. J. and Fekete, D. M. (2009). Mapping of Wnt, frizzled, and Wnt inhibitor gene expression domains in the avian otic primordium. *J. Comp. Neurol.* **517**, 751-764.
Stevenson, B., Mayor, R. and Streit, A. (2012). Mutual repression between Gbx2 and Otx2 in sensory placodes reveals a general mechanism for ectodermal patterning. *Dev. Biol.* **367**, 55-65.
Streit, A. (2002). Extensive cell movements accompany formation of the otic placode. *Dev. Biol.* **249**, 237-254.
Vaage, S. (1969). The segmentation of the primitive neural tube in chick embryos (Gallus domesticus). A morphological, histochemical and autoradiographical investigation. *Ergeb. Anat. Entwicklungsgesch.* **41**, 3-87.
Washausen, S., Obermayer, B., Brunnett, G., Kuhn, H.-J. and Knabe, W. (2005). Apoptosis and proliferation in developing, mature, and regressing epibranchial placodes. *Dev. Biol.* **278**, 86-102.
Whitfield, T. T. and Hammond, K. L. (2007). Axial patterning in the developing vertebrate inner ear. *Int. J. Dev. Biol.* **51**, 507-520.
Wu, D. K., Nunes, F. D. and Choo, D. (1998). Axial specification for sensory organs versus non-sensory structures of the chicken inner ear. *Development* **125**, 11-20.
Xu, H., Dude, C. M. and Baker, C. V. H. (2008). Fine-grained fate maps for the ophthalmic and maxillomandibular trigeminal placodes in the chick embryo. *Dev. Biol.* **317**, 174-186.
Yang, L., O'Neill, P., Martin, K., Maass, J. C., Vassilev, V., Ladher, R. and Groves, A. K. (2013). Analysis of FGF-dependent and FGF-independent pathways in otic placode induction. *PLoS ONE* **8**, e55011.